



JOURNAL OF SPATIAL INFORMATION SCIENCE  
Number 12 (2016), pp. 87–111

doi:10.5311/JOSIS.2016.12.261

RESEARCH ARTICLE

# Exploring the human body space: A geographical information system based anatomical atlas

Antonio Barbeito<sup>1</sup>, Marco Painho<sup>2</sup>,  
Pedro Cabral<sup>2</sup>, and João Goyri O'Neill<sup>3</sup>

<sup>1</sup>School of Technology and Management of Águeda, University of Aveiro, Portugal

<sup>2</sup>NOVA IMS, Universidade Nova de Lisboa, Portugal

<sup>3</sup>NOVA Medical School, Faculdade de Ciências Médicas, Universidade Nova de Lisboa, Portugal

*Received: October 12, 2015; returned: January 27, 2016; revised: March 11, 2016; accepted: April 5, 2016.*

---

**Abstract:** Anatomical atlases allow mapping the anatomical structures of the human body. Early versions of these systems consisted of analogical representations with informative text and labeled images of the human body. With computer systems, digital versions emerged and the third and fourth dimensions were introduced. Consequently, these systems increased their efficiency, allowing more realistic visualizations with improved interactivity and functionality. The 4D atlases allow modeling changes over time on the structures represented. The anatomical atlases based on geographic information system (GIS) environments allow the creation of platforms with a high degree of interactivity and new tools to explore and analyze the human body. In this study we expand the functions of a human body representation system by creating new vector data, topology, functions, and an improved user interface. The new prototype emulates a 3D GIS with a topological model of the human body, replicates the information provided by anatomical atlases, and provides a higher level of functionality and interactivity. At this stage, the developed system is intended to be used as an educational tool and integrates into the same interface the typical representations of surface and sectional atlases.

**Keywords:** 3D GIS, human body model, topology, spatial analysis, anatomical atlases

---

## 1 Introduction

Anatomical atlases aid the study of the human anatomy by providing pictorial information associated with descriptive texts [33]. The current analogic anatomical atlases have evolved considerably with regard to detail, accuracy, and visual quality. The advent of three-dimensional (3D) [46] models made it possible to build new atlases with greater study and interaction capabilities [8]. The development of 3D atlases in digital format allows the representation with greater realism and detail of the anatomical structures and also enables the completion of identification operations, spatial analysis, and measurements. There is a wide variety of anatomical atlases that differ as to the forms of representation, the specific field of study, and the set of anatomical structures described. Atlas [16] and atlas [53] illustrate two different ways of representing anatomical information: the first is an atlas of sectional anatomy, in which the human body is viewed through axial images; and the second is based on surface anatomy, in which one can see the outer surface of the structures with the possibility of generating stereo views.

Many imaging techniques allow adding information to the usual traditional content through the inclusion of images of different types, e.g., computed tomography (CT), magnetic resonance imaging (MRI), and cryosection red green blue (RGB) images [1]. Another possibility is to develop atlases based on data generated by imagiology [39]. In addition to the atlases that provide global representations of the human body, there are others whose representation focuses on some specific structures [27]. Currently, there are available on the internet three-dimensional systems based on surface anatomy, whose information is organized in layers and that provide interactive tools that explore the respective models [2, 6, 14, 54].

4D digital atlases cover the spatial (3D) and time (1D) dimensions, allowing studies in which changes over time are sought. The eMouse Atlas Project (EMAP) [35] is based on a detailed model of the developing mouse. The EMAP system integrates spatial, temporal, and anatomical data, allowing powerful computational analyses. Similar to GIS models, it has topological information, namely, a detailed anatomy ontology that gives the names and structural relationships between the parts [20]. The EMAP is intended to be used as an educational or research tool.

GIS were conceived to operate with spatial information and usually contain topological models that are particularly suited to implement and perform spatial analyses. With the growing need of modeling three-dimensional environments [3, 23], research in GIS models and systems has been dedicated to 3D. 3D GIS spatial data models fall into two categories: surface data models and solid data models [24]. The first are usually implemented with vector components. The second, also known as volume models, are based on vector (e.g., the tetrahedral network, TEN, model [32]) or raster components. Both models are implemented to represent environments in which there are human constructions and natural objects, such as the Earth's surface and the geological structures beneath it. In fact, in environments where it is necessary to perform surface and volume representations simultaneously, it is advantageous to merge the two models into a single integrated model [42].

Currently the models available in 3D GIS are not as developed and tested as the 2D GIS models. The transition from 2D to 3D systems implies the representation of more complex objects [7]. The existing 3D GIS models have been developed to represent specific objects and there does not yet exist a generic, overall model.

The most usual applications of GIS in health refer to the relationship between diseases and geographic space, namely, epidemiological studies. The relevance of GIS in these studies is demonstrated in [31, 34]. Although unusual, the association of GIS to anatomical structures modeling has been the subject of some research. The study [18] explains the advantages of the visualization and spatial analysis of clinical data as a result of rendering anatomical and pathological features in GIS. Several studies have modeled the mouse brain. The Smart Atlas, developed under the Biomedical Informatics Research Network (BIRN) project, creates a spatial database to store information and to perform queries on data from an atlas of the mouse brain [26]. This system is a truly GIS-based atlas environment enabling users to discover, access, visualize, and query heterogeneous images and image markup [51]. Representations of the human brain are also available, along with the tools developed that allow interacting with the model.

Even so, the lack of three-dimensional topological data models specifically designed and tested to represent the human body in GIS [41] and the interest of this representation [44], calls for the need for research in this area.

The integrated model introduced in [4] and developed in [5], here referred to as the input model, takes advantage of GIS graphical environment and functionalities to give typical information of anatomical atlases. This model also provides new features and functionalities that increase the possibilities of analysis of human anatomical structures, such as visualizing the interior of the anatomical structures by setting cutting planes and identifying structures on the raster component. This model is part of a group of representations that provide realistic visual information from the interior of anatomical structures by using the data available from the Visible Human projects [29, 38, 52]. In addition to the visual aspect of the representation, these systems provide functionalities related to the objectives for which they were developed, in particular, the visual exploration of the human body and the identification of anatomical structures.

In this paper we implement a prototype of an anatomical atlas of the human body in a GIS environment, with emphasis on the expansion of the topological component model and on the development of features that enhance the system capabilities. The new topological component results from the expansion of neighborhood topology and from the creation of a new connectivity topology. The GIS features to be applied should include not only the three-dimensional visualization capabilities, but also the ability to manipulate and analyze 3D data, adding functionalities that are unusually provided by the existing anatomical atlases.

The features of the expanded system include:

1. The tools developed in previous implementations [4, 5]:

(i) An interface to explore and identify the input images directly; (ii) navigation functions; (iii) identification functions to explore the 3D model; (iv) information management through a TOC that lists all the anatomical structures contained in the system; (v) spatial analysis functions based on forms of topology developed in the model: containment and neighborhood; (vi) cutting planes setting tool to view the interior of anatomical structures; (vii) a tool for simulating the insertion-of-a-needle; (viii) visualization of raster and vector components with two types of color: simulated color, for structural sets and segmentation color, for each structure.

2. The tools developed in the present work, some of which became possible from the improvements made in the present model:

(i) A module to explore the RGB input images directly; (ii) editing functionality for updating detailed information about the anatomical structures represented; (iii) added identification functions with different levels of detail; (iv) improvement of the TOC through a layer system that translates a hierarchical classification scheme of the anatomical structures; (v) improved neighborhood analysis function based on the expanded neighborhood topology; (vi) measuring tools (made possible through the implementation of a real coordinate system): linear (including connectivity topology in the model allows doing this kind of measuring on structures that have branches), superficial, and volumetric; (vii) visualization of raster and vector components with true color.

## 2 Methods

### 2.1 Data

The system developed in this work results from the expansion of the models presented in [4, 5]. This system contains an integrated model of the human body and uses CT and cryosectional (RGB) images of one male human body from the Visible Human Project (VHP). These images provide information on the internal anatomical structures and allow building 3D vector surface objects that represent its boundaries. For each anatomical structure, corresponding to an information layer, the geometric component of the input model is composed of a surface triangle mesh (vector component), connected to the respective volumetry in raster format, which is contained in the layer matrix (LM) via a common identifier (ID). The LM is a voxel matrix that stores the segmentation information of the anatomical structures whose true color information is in the RGB input images.

The topological components of the model describe the containment information through the LM matrix and neighborhood, through a table of structures containing for each structure the identification of nearby structures.

### 2.2 Input model expansion

The changes operated in the input model include: the implementation of connectivity topology, the association of neighborhood topological information and true color to each vertex of the vector component, and the building of a geometric component formed by the central axes structures that evolve linearly in space (Figure 1). The remaining developments concern new implemented functionalities, some of which use the new features of the model.

The linear structures implemented in the expanded model do not have physical correspondence with the anatomical structures of the human body. These representations are common in GIS and are associated with objects that evolve linearly in space. These structures enable length measurements and network analysis operations, such as determining optimal paths. In the expanded model, the structures that evolve linearly, such as blood vessels, have a center line corresponding to the central axis of the structure in three-dimensional space. The branches of the structure are linked by nodes.

To create the central axes, the repulsive potential method was used [11]. After obtaining the axes, the points are filtered and reconstructed to have a homogeneous distance with a comparable size to the resolution of the input data (VHP images).

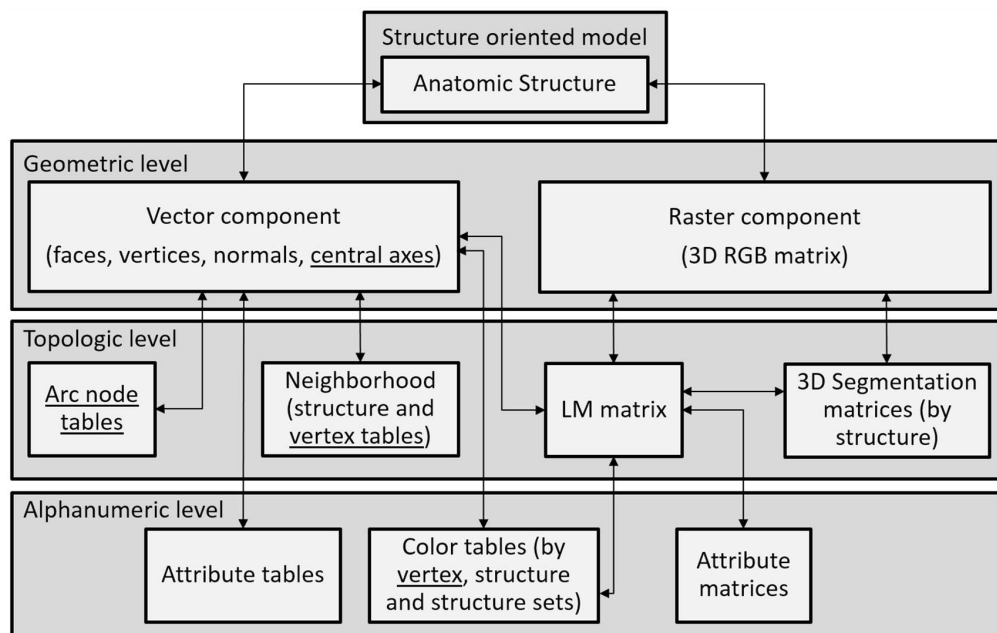


Figure 1: Expanded model. The new components that expand the model are underlined.

This procedure was followed for the blood vessels. However, it is not efficient in the case of the intestines, which are structures that fold over themselves and have large compression zones. In this case, the vector surface structure does not represent the real anatomical surface, and determining the central axis depends on an incorrect structure. In this particular case we have developed a manual module that allows the user to place the points of the central axis in images using different perspectives: the original axial images and the front vertical images. Thus, it is possible to reconstruct the points corresponding to the central axis. The last point closes the sequence, enabling the reconstruction of the central axis structure.

The topological component associated with the central axes is defined explicitly in the model through arc-node tables, in which each record contains the start and end nodes and the impedance—in this case, the length—of each arc that composes the central axis.

As is typical in GIS, the neighborhood topological component was developed by scanning the spatial components of the model, in this case, the vector components of the anatomical structures. With this information each anatomical structure knows its neighboring structures. The expansion performed in this topological component consists of bringing this knowledge to each vertex of the vector component that forms the surface of the anatomical structures. Thus, the neighborhood analysis can be applied to a sub-region of an anatomical structure and not only to the entire structure.

The procedure consists of recording, for each vertex of the surface vector component of each anatomical structure, the vertices of the neighboring structures, i.e., the vertices of the structures with a different ID, placed at a distance similar to the largest dimension of

the raster data component. The IDs of the neighboring structures found are stored in the model structure after eliminating repeated values.

### 2.3 Classification of anatomical structures and multilayer management

The management of a layer information system through a table of contents (TOC) available in the graphical interface is common in GIS applications. The input model is available in a system of this type in which the anatomical structures are listed alphabetically in the TOC. The manipulation of information in the TOC consists of enabling/disabling the listed anatomical structures. In this work, the management of anatomical structures has been improved to reproduce typical classifications in anatomical atlases. Thus, three hierarchical classification systems based on regions, tissues, and systems were included [43]. The classification systems, thoroughly described in spreadsheets, were converted into binary files and imported into the file structure of the prototype, and are implemented in the TOC of the graphical interface whenever the application is run.

### 2.4 Reference system

The input model and the respective interface do not provide measurement capabilities. In that interface, the reference system and the model dimensions do not correspond to the actual dimensions. With the inclusion of measurement tools in the expanded model, it became necessary to assign the actual dimensions. To this end, the coordinates of the original image data were converted into real coordinates in the final model. The vector surface of the body was used to determine the three-dimensional coordinate system: the system origin was the centroid of all vertices coordinates of this component.

Several studies [25, 26, 30, 50, 51] have defined and used coordinate systems to reference anatomical structures. With regard to the present model, the real coordinates are already contained in the parameters of the input image data, thus, converting this first coordinate system, through the provided parameters, allows obtaining the intended 3D reference system. The horizontal coordinates were determined as a function of the horizontal resolution of the images, i.e., 0.33 mm per pixel in  $X$  and  $Y$ . The vertical coordinates took into account the distance of 1 mm between every two successive images. The system orientation was defined according to the sagittal, coronal, and axial planes, as is usual in human body representations. The definition of a direct coordinate system with the  $Z$  axis increasing in the caudal-cranial direction is achieved by reverting the direction of  $Y$  and  $Z$  axes in relation to input images (Figure 2).

### 2.5 Spatial visualization

The input model enables the display of the raster and vector components in different color records. The raster component—showing the internal structures through cutting planes—can be viewed in true color through the RGB images of the original data or by the segmentation color defined in the LM which assigns each segmented anatomical structure to a single color. This component can also be displayed after three-dimensional reconstruction of voxels with true color information [10, 48].

The three-dimensional visualization of segmented structures through the vector surface components can use the segmentation color of the LM matrix or another false color similar



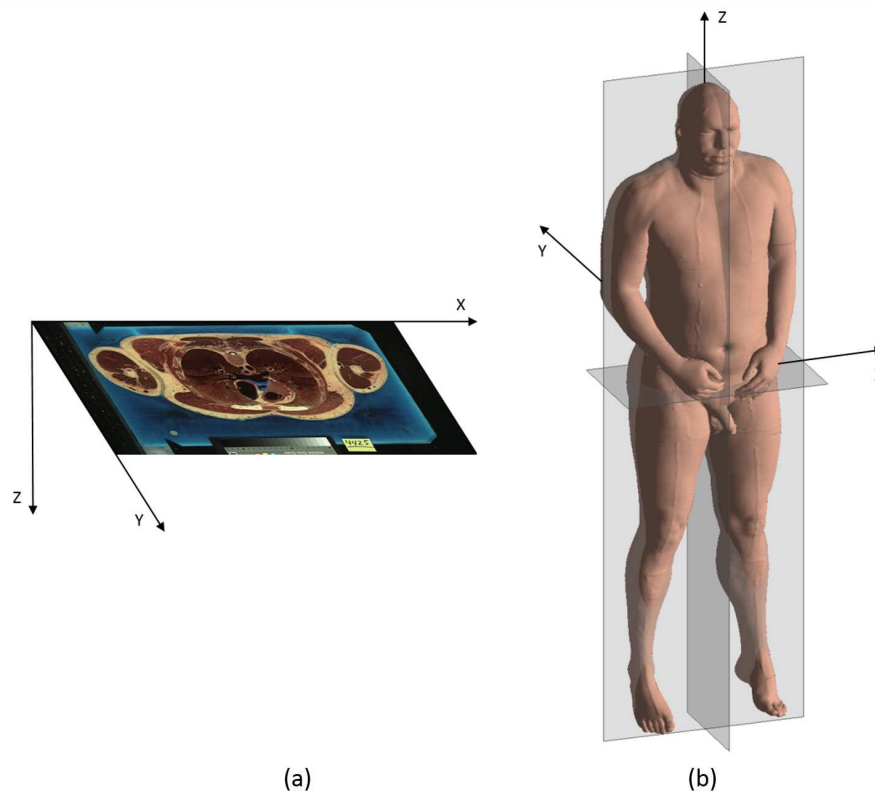


Figure 2: Coordinate systems. (a) Coordinates of input image data; (b) Three-dimensional coordinates defined using the vector model of the human body surface.

to the one of the represented structures. This color aggregates groups of structures, for example, a color for all the muscles and another one for all the bones. In the original model one can visualize the raster component with false or true color, but when it comes to the three-dimensional reconstruction of a given structure through the vector component, there is only false color information.

To introduce true color information in this model, the following procedure was developed: for each vertex of the vector components, the RGB value of the nearest voxel is recorded. This record is stored in the model structure, being associated with the corresponding anatomical structure, and this texture map is used to render the surface vector component with true color information. In reality, the true color information is approximate because the RGB values used to render the faces of the vector components do not necessarily correspond to the boundary voxels of the corresponding structures. However, the rendering of the vector component with the resulting color information allows visualizing the anatomical structures with a more realistic appearance when compared with false color.

The definition of the cutting planes for viewing the interior of the body is defined in the input model. This definition can be carried out by simulating the insertion of a needle

into the body surface. In the current model, this feature uses the multilayer characteristics to implement the definition of cutting planes from the insertion of a needle in different anatomical structures, and not just on the body surface. The mechanism is analogous to the initial model, in which the definition of a cutting plane started with a given point on a structure that is simultaneously identified. The orientation of the needle defines the cutting plane on the identified structure. Then, the algorithm is applied that makes the detection, cutting, and reshaping of the triangles of the vector component, as well as the rendering of the cutting plane, with raster information representative of the internal structures.

## 2.6 Measurement tools

Once the actual real coordinate system was implemented, four measurement functions were developed: area, volume, length between two points, and length between two points along a structure. These operations were constructed to benefit from the features of an integrated topological model. In this sense, it becomes possible to simplify certain measuring algorithms using the information available in the model: (i) measuring areas consists of determining the surface area of a given anatomical structure. This operation is associated with the vector component surface, in which the calculation made from the sum of the areas of the triangles that form the surface of the structure; (ii) measuring volume uses the raster component and consists of counting the voxels of the anatomical structure. The conversion to volume is based on multiplying the number of voxels by its known volume ( $1 \times 0.33 \times 0.33 \text{ mm}^3$ ); (iii) measuring lengths along an anatomical structure is based on the topological connectivity information of the linear component of the model. To perform this type of measurement, the points along which it is intended to measure the length of the anatomical structure are selected. After selecting the points, situated on the component of the central axis of the structure, the reading of the topological component described in arc-node table, allows to calculate the total impedance—the desired distance—using the Dijkstra's algorithm [15, 21]; (iv) measuring lengths between two points consists of calculating the Euclidean distance in the usual way in a three dimensional space. This distance depends exclusively of the coordinates of the two given points, and does not use the characteristics of any of the components of the model.

The four developed measurement functionalities are available in the graphical interface and work interactively with the placement of measurement points on the structures.

## 2.7 Identification and editing

The identification function provides the names of the anatomical structures at the internal and surface raster component levels. After the interactive selection of a point on the model, its coordinates are determined for identifying the anatomical structure to which it belongs. In this way, a point selected interactively returns a label with the name of the respective structure.

In the current model two features associated with the identification of sub-regions in the surface vector component of an anatomical structure were developed. The first functionality corresponds to the edit mode. When activated, it assigns a name and colors over the surface component of an anatomical structure, the region corresponding to the defined name.



Once this level of information is created, the second functionality, the identification function, allows for extracting this information and displaying it in the same way as the identification function.

### 3 Results and discussion

#### 3.1 Inclusion of central axes and connectivity topology

The implementation of the connectivity topology is associated with the inclusion of central axes in some anatomical structures. The definition of the axes is made via an interactive application that generates three different views of the input data: (i) the original axial images; (ii) front vertical images of the same data; (iii) a three-dimensional image that enables the visualization of the voxels of the anatomical structure with a degree of transparency dynamically defined by the user (Figure 3). In both of the input images, the cursor must be positioned in the center of the structure. The cursor appears in the three-dimensional image, and it is possible to confirm the position within the structure. After determining all the positions, the central axis is defined and registered in the model structure by creating the topology arc-node table that is associated with the ID of the corresponding anatomical structure.

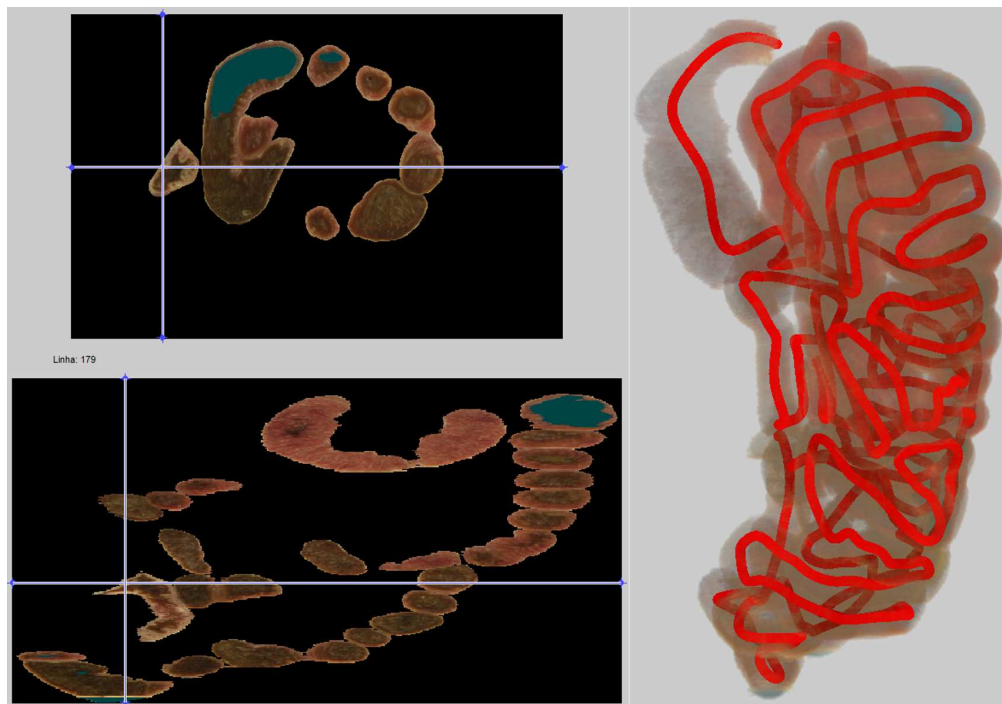


Figure 3: Interactive interface in which the central axes of the anatomical structures is defined.

### 3.2 Classification of anatomical structures and multilayer management

The management of the display of the model structures is made through the table of contents (TOC). The alphabetical listing of anatomical structures in the TOC is not the most efficient way to manage the information layers. An alternative way of presenting the TOC is to rank the anatomical structures as is usual in the anatomical atlas. This obtains a more efficient organization scheme and faster access to each structure or groups of structures. To implement classification systems in the graphical interface, three different hierarchical forms were added to the TOC that enable the organization of the anatomical structures in regions, tissues, or systems. The different classifications are exclusive and when one of the classifications is selected the TOC is filled with the corresponding hierarchical tree (Figure 4).

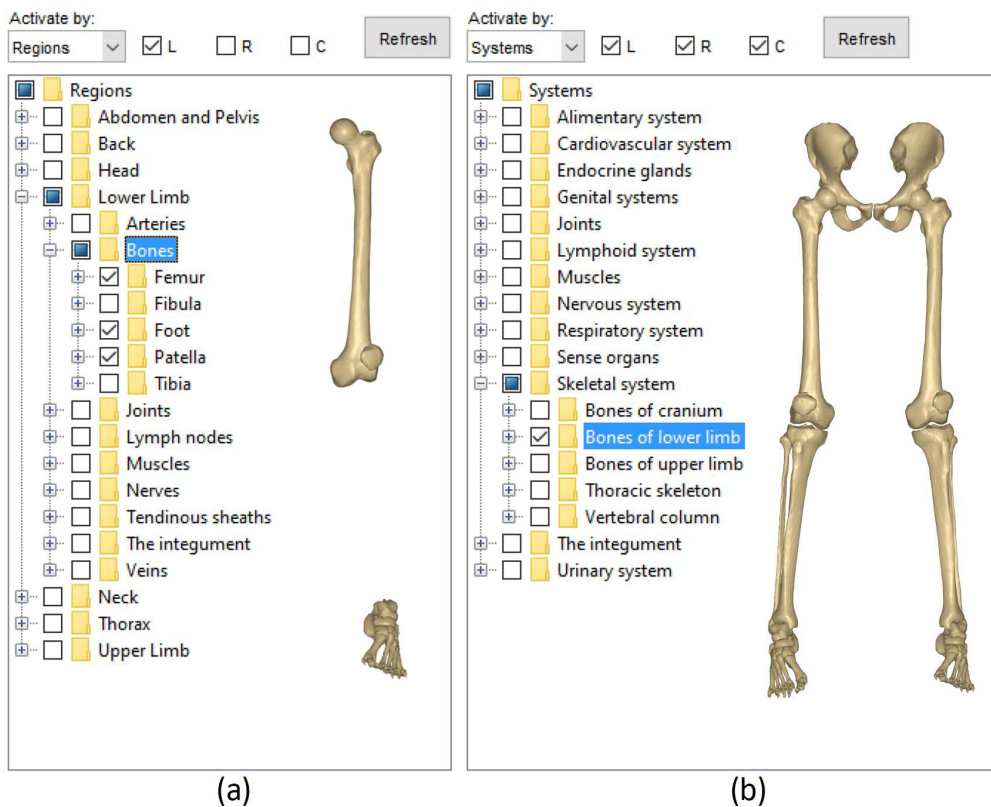


Figure 4: Hierarchical classification systems implemented in the TOC. (a) Classification by regions; (b) Classification by systems.

### 3.3 Input data exploration

In the prototype, the most direct access to input data is through the application shown in Figure 5. This application allows a direct operation of the input data. In the region on the

right an image is selected through its positioning in the human body, which is shown on the left. The identification function is included in this application.

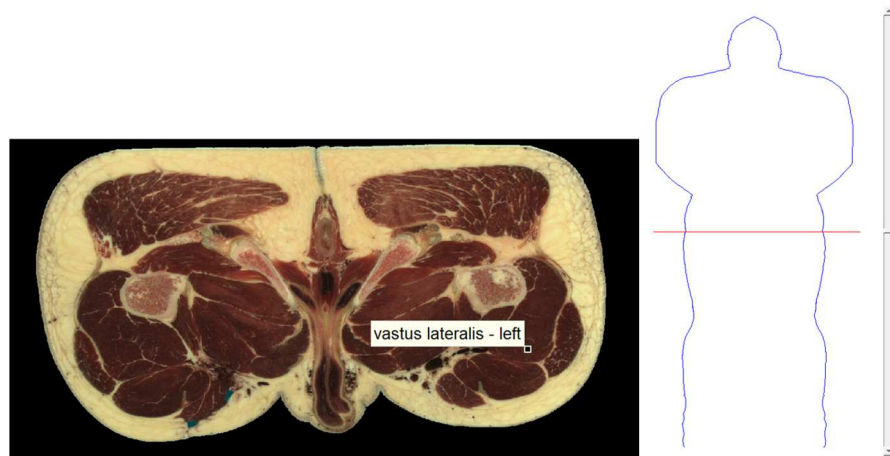


Figure 5: Input data direct exploration and identification function.

### 3.4 Spatial visualization

GIS offer 2D or 3D maps in their graphical interfaces. In the present system, a model of the human body is mapped in a three dimensional space. The forms of visualization of this map are very important features because the adequate communication of information relies on them. To this end, different types of visualization aiming to communicate different aspects of information were implemented, namely, (i) the visualization of internal component in true color (the color in the RGB input images); (ii) the display of the internal component with the segmentation color (contained in the LM matrix); (iii) the display of the vector component in false color (a simulated color for a group of structures, for example, one color for bones and another color for muscles); (iv) the display of surface component in the segmentation color (a color for each segmented structure); (v) the surface texturing component with true color information, and (vi) the display of three-dimensional raster structures in format voxel. Figure 6 illustrates some of these display methods.

The input model included a function that allowed defining cutting planes from the insertion of a needle. The needle could be inserted in any point of the surface of the body and according to the depth of the needle insertion and orientation the cutting plane was determined in order to correspond to the line of maximum slope. Figure 7 shows the result of this type of cutting plane setting, now extended to insert the needle into any predetermined structure.

### 3.5 Neighborhood topological component expansion

Since the model was initially built from transverse images of the body, the neighborhood topological information could be determined from the segmenting polygons drawn around the anatomical structures on these images. However, this approach can lead to a loss of

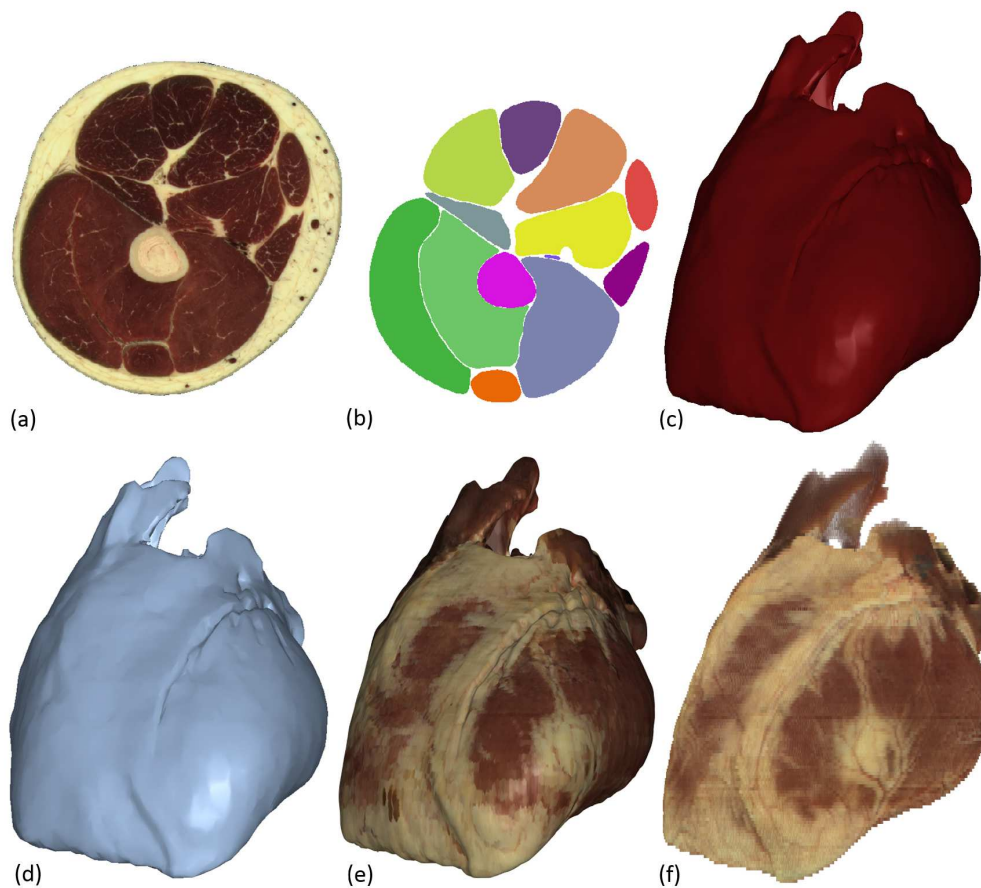


Figure 6: Spatial visualization modes available in the system. (a) True color on the raster component; (b) Segmentation color on the raster component; (c) False color on the vector component; (d) Segmentation color on the vector component; (e) Color obtained by texturing the vector component; (f) Three-dimensional raster component with true color.

relationships between objects that meet along the vertical direction. Thus, the 3D vector components of the model are used to retrieve the neighborhood topological information. It should be noted that the neighborhood topological tables are built only from the contained structures, which, for the lower limb, include the muscles and the bones. When more structures are segmented and included in the model, this topological information becomes more complete and the analysis more accurate.

With the topological neighborhood information available, it becomes possible to determine the structures in the neighborhood of a sub-region of a predefined structure. Table 1 shows the neighboring muscles of the femur: in the first column, the analysis is made to the whole structure, and in the second to the upper half of the bone. By analyzing this table it can be seen that the short head of biceps femoris is taken from the result of the second

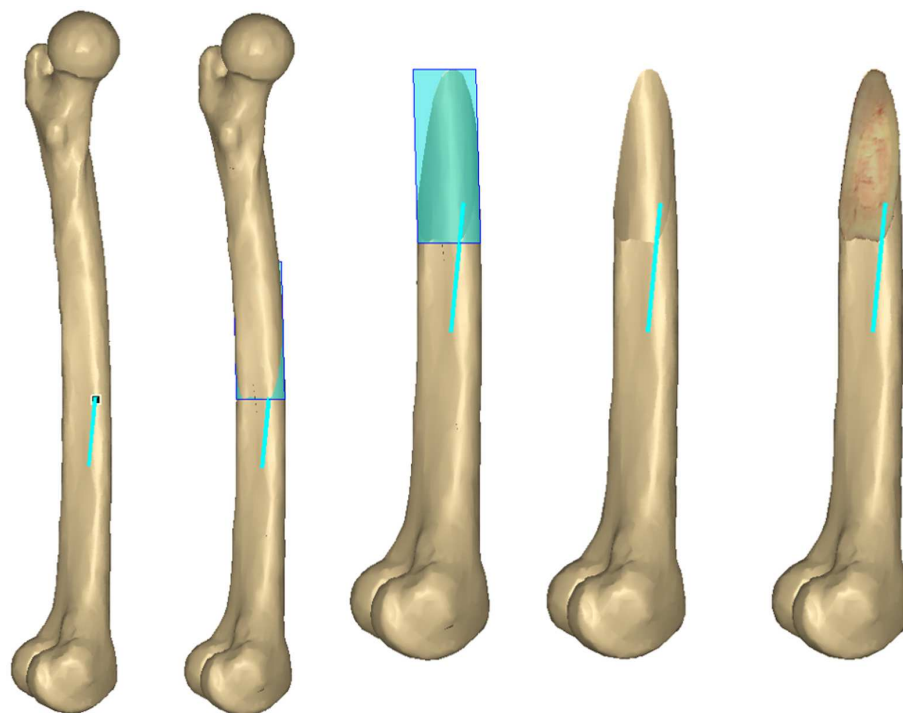


Figure 7: Application of a cutting plane from the interactive insertion of a needle.

analysis. The position of this structure relative to the femur is shown in Figure 8, where it can be seen that it is not neighboring the upper half of the femur.

Muscles adjacent to the femur	Muscles adjacent to the upper half of the femur
adductor brevis, adductor magnus, gluteus medius, obturator externus, quadratus femoris, short head of the biceps femoris, vastus intermedius, vastus lateralis, vastus medialis	adductor brevis, adductor magnus, gluteus medius, obturator externus, quadratus femoris, vastus intermedius, vastus lateralis, vastus medialis

Table 1: Spatial neighborhood analysis: Determination of the left leg muscles that are neighbors of the total and the top half of the femur.

The neighborhood topology allows for responding adequately to neighborhood analysis carried out on this particular model. The use of this information jointly with a theoretical neighborhood model (not included in the present system), allows for detecting possible deviations in the anatomical model represented



Figure 8: Neighborhood analysis. The neighborhood analysis detects that the short head of the biceps femoris is not neighboring the upper half of the femur.

### 3.6 Measurement tools

The metric functions implemented in the prototype were assessed by comparing the results with reference values available in scientific studies. These tests cannot rigorously assess the precision of these tools. However, they are a good indicator if they are consistent with the values reported in the literature. For the VHP male model, height and weight are, respectively, 186 cm and 104 kg [9]. Both the height and weight are measures usually obtained in the calculation of common ratios in anthropometry works and will be used in some of the checks made. The height and weight of the VHP model lead to a body mass index (BMI) [49] value of  $30.1 \text{ kg/m}^2$ , which corresponds to an obese condition.

Figure 9 illustrates measurements that use the various metrics tools provided by the system.

Of all the metrics features used, measuring the distance between two points is the only one that does not use model-specific features. This measurement was tested over the left femur and compared with reference values. The length obtained on the model was 48.3 cm. In the study presented by [17], carried out on a sample of 13,149 individuals, comprising 51 populations from different geographic areas, the mean value obtained for the femur/height ratio was 26.74%. Thus, the following formula, which relates the length of the femur with height of an individual, is proposed (1):

$$\text{Height} = \text{femur length}/0.2674 \text{ (cm)} \quad (1)$$

The height calculated by this expression, from the femur length of the value obtained on the model, is approximately 181 cm, which corresponds to a deviation of less than 3% of the actual height of the model. In the study [40] the tibiofemoral relationship is evaluated. With 378 measurements a ratio of 1 to  $1.26 \pm 0.1$  was obtained. The measurement of the left tibia in the model was 40.19 cm, resulting in a femur/tibia ratio of 1.2. This value falls within the range obtained in this work.



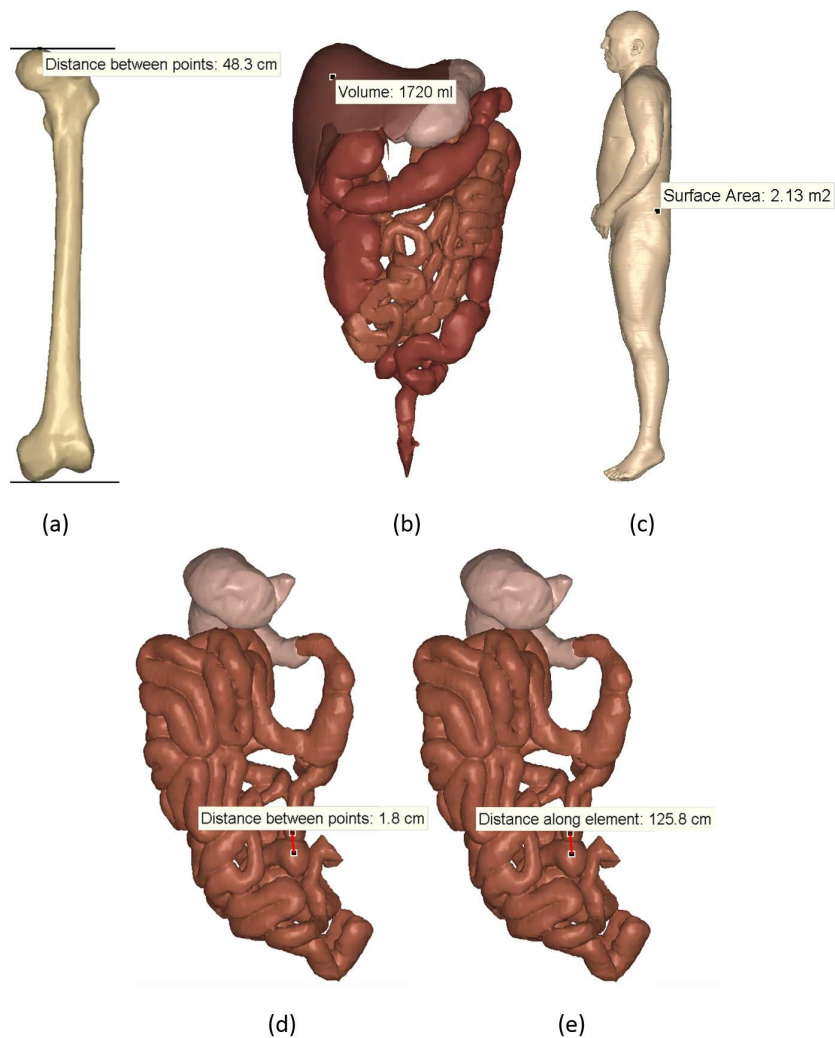


Figure 9: Measurements of anatomical structures. (a) Measuring the distance between two points; (b) Determination of the liver volume; (c) Measurement of the surface area of the human body; (d) Measuring the distance between two points in the small intestine; (e) Measurement of the distance between two points along the small intestine.

The volume of the liver and the stomach were determined using the model. Volume of the liver was 1720 ml, in which the weight/volume ratio was equal to 60.5 kg/l. In the study [22], with 22 volunteers without clinical or laboratory evidence of liver disease, estimates were obtained from images generated by single-photon emission computed tomography (SPECT) for this ratio. An average value of 43 kg/l with a standard deviation of 5 kg/l was obtained for the male volunteers. This value does not frame the ratio obtained with the measuring tools of the prototype. In this case the comparison should take into account the obese condition of the prototype model. In fact, only two of the male volunteers in the

study have an overweight condition. In particular, the volunteer that has the higher BMI value,  $26.3 \text{ kg/m}^2$ , presents the closest ratio,  $53.1 \text{ kg/l}$ , to the one found in the model. The liver volume/body area ratio ( $\text{l/m}^2$ ) calculated on the same sample, shows a mean value of  $0.891/\text{m}^2$  with a standard deviation of  $0.081/\text{m}^2$ . Using the tools to measure the liver volume and the body surface area of the model, the value obtained was  $0.811/\text{m}^2$ .

For the stomach, the references to its volume have a considerable variability. The studies [13, 36, 47] indicate a maximum value of 400 ml. In the context of morbid obesity (BMI higher than  $40 \text{ kg/m}^2$ ), the study [12] found values for stomach volume from 850 ml. The measurement performed on the model resulted in a value of 465 ml.

To evaluate the area measurement tool, the body surface area (BSA) was determined on the model, obtaining the value of  $2.13 \text{ m}^2$ . This value was compared with those obtained by three expressions that were introduced on separate occasions. The three expressions use the height (cm) and the weight (kg) of the body and return the value in  $\text{m}^2$ :

$$\text{Du Bois formula [19]: } BSA = 0.007184 \times \text{Weight}^{0.425} \times \text{Height}^{0.725} \quad (2)$$

$$\text{Mosteller formula [28]: } BSA = \sqrt{\frac{\text{Weight} \times \text{Height}}{3600}} \quad (3)$$

$$\text{Schlich formula (male version) [37]: } BSA = 0.000579479 \times \text{Weight}^{0.38} \times \text{Height}^{1.24} \quad (4)$$

The BSA values obtained for the VHP model according to the expressions (2), (3) and (4) were, respectively,  $2.72 \text{ m}^2$ ,  $3.02 \text{ m}^2$ , and  $1.92 \text{ m}^2$ . Beyond these empirical expressions that lead to a wide range of values, we used another study as reference [45], which gives intervals around the mean BSA values. This study is based on 1868 patients who were classified into three groups, considering the BMI values: (i) normal group  $23 \pm 1 \text{ kg/m}^2$ ; (ii) overweight group,  $27 \pm 1 \text{ kg/m}^2$ ; (iii) obese group,  $27 \pm 1 \text{ kg/m}^2$ . The BSA global value was  $2.04 \pm 12.24 \text{ m}^2$ :  $1.81 \pm 12.19 \text{ m}^2$  in the normal group,  $1.99 \pm 12.16 \text{ m}^2$  in the overweight group, and  $2.21 \pm 0.22 \text{ m}^2$  in the obese group. Comparing the measured value with the global values of the study and with the overweight group, there is, once again, a correspondence between the measurement and the study values.

The measurement along a branched structure allows validating not only the metrics tool, but also the model connectivity topology component. Figure 10 shows a measurement performed on a set of arteries that have a branch at the abdominal aorta and the common iliac arteries level. The application of Dijkstra's algorithm to the arc-node table allows finding the path between the two data points and determining the total length between them.

### 3.7 Editing and identification

The editing and detail identification functionalities are shown in Figure 11. The editing functionality begins with the assignment of the region name, followed by its definition on the three-dimensional geometric component through a painting tool. Once the delineated region is accepted, the information becomes available in the detail identification function. By creating alternative levels of information, this tool allows not only identifying anatomical sub-regions on an anatomical structure surface, but also assigning other attributes to these sub-regions as required by the user.

The identification tool is available for all the data in the user interface (UI). Thus, beyond the identification performed on the surface of the anatomical structures, as shown in



Figure 10: Measurement of length between two points on a set of arteries. (a) Arteries view (aortic arch, thoracic aorta, abdominal aorta, common iliac artery, external iliac artery, femoral artery); (b) Central axis of a set of arteries represented with a measurement.

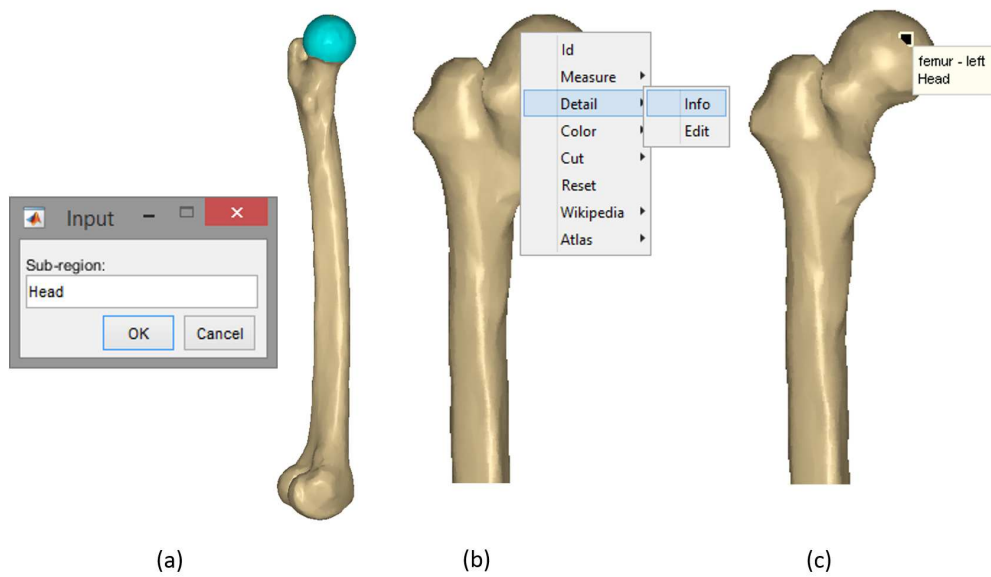


Figure 11: Editing function and detail identification. (a) Creation of a sub-region in an anatomical structure; (b) Enabling the detail identification function; (c) Applying the detailed identification.

Figure 11, the same tool can be used on the raster data (Figure 12). The identification tool shows names, pages of local documents, or internet pages about the requested structures.

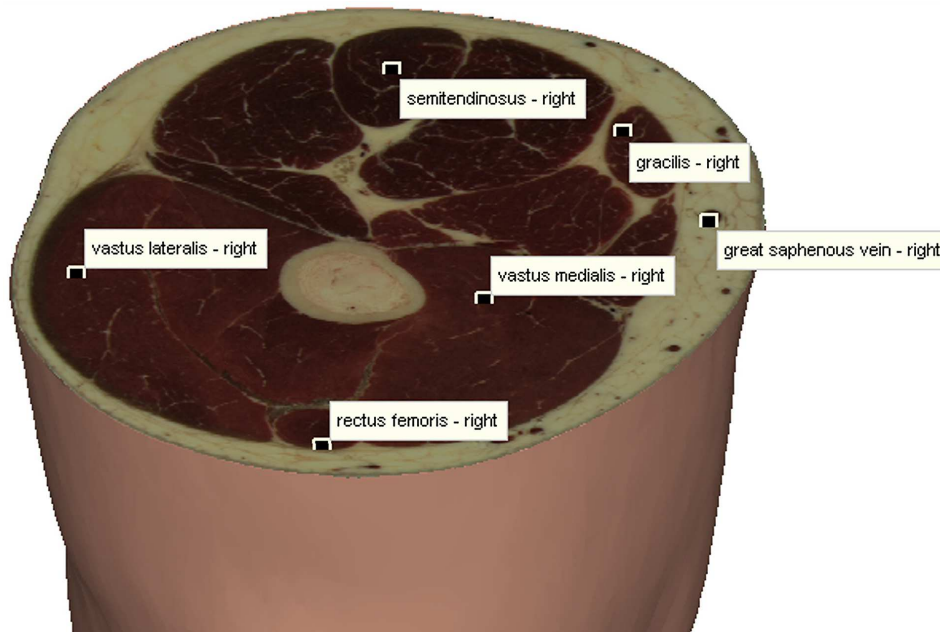


Figure 12: Identification tool used on the raster data.

### 3.8 Interactive operation in 3D environment

The earlier sections described the tools and the model improvements made in the prototype. However, the description of the tools, in itself, overlooks some of the advantageous aspects of the prototype as an anatomical atlas of the human body. With this perspective, some features of the prototype will be mentioned together in this section to better explain the possibilities of the prototype in the exploitation of the anatomical structures. To this end, the data integration, the cut and reconstruction tools, the analysis ability (namely, the inclusion analysis), and the interactive use of all these aspects in a 3D environment, are specifically mentioned to show the possibilities of the present system.

The model included in the prototype has true 3D vector components representing the surfaces of the anatomical structures (non-convex polyhedra constituted by a mesh of triangles). In turn, each 3D vector part is uniquely linked to its interior raster data. All these components are represented in a 3D interface that offers interactive tools. Thus, the functions of the system that interact with the anatomical model (e.g., identification, navigation, measurements, and spatial analysis) run in a 3D environment. The possibility to cut and reconstruct anatomical structures, in a sequential procedure, allows exploring its interior and, simultaneously, observing its real (3D) morphological configuration. Additionally, the layer system allows applying the tools for specific structures (Figure 13).

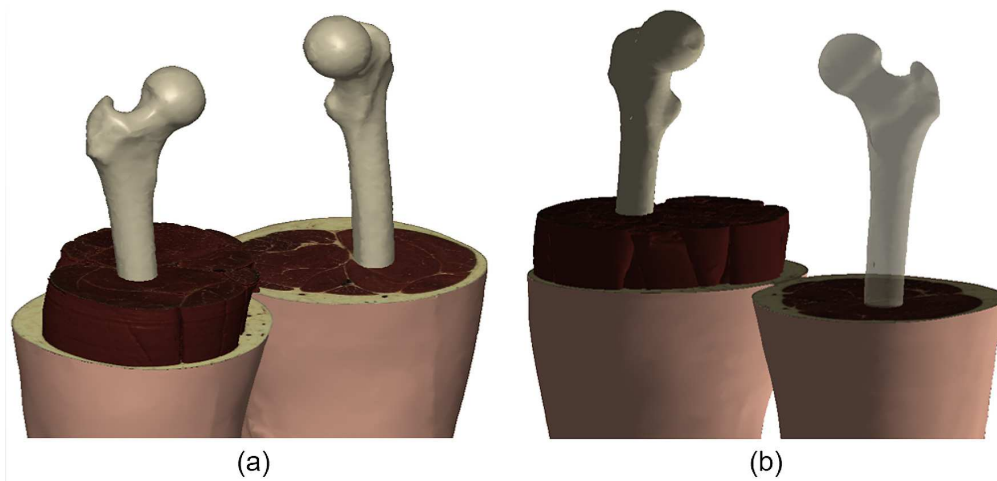


Figure 13: Integration of vector and raster data and applying interactive tools in the 3D UI. (a) Sequence of interactive operations: Applying a cutting plane in the surface of the body; reconstructing the muscles of one leg; applying a new cutting plane to the reconstructed muscles; reconstructing the femur of the two legs; (b) Applying a certain degree of transparency to a specific data layer.

The prototype tools run on 3D data models. When compared with 2D GIS, 3D GIS present some limitations in terms of available tools. In 2D GIS the inclusion analysis is done through “point-in-polygon” algorithms.

In 3D GIS, usually, the inclusion analysis is used to find if a point is above or below the Earth’s surface. In 2D or 2.5D GIS, to carry out this kind of analysis, the “point-in-polygon” algorithms are largely used. However, they are not very useful in 3D because they run only with polygons (2D). If a 3D model relies only on vector data, the use of “point-in-polyhedron” algorithms becomes necessary. However, if the model links vector surface components to its interior in raster format, the inclusion analysis becomes simpler. In this case, the adequate connection between the two components allows performing an inclusion analysis by simply reading the raster component derived from the connection vector-raster, named LM matrix in section 2.1. Figure 14 depicts an example of inclusion analysis with the multilayered structured data. The analysis consists of determining the structures crossed by a needle. After the interactive insertion of the needle, a cutting plane is generated. The orientation the needle is the steepest direction of the cutting plane. The crossed anatomical structures are then encoded on the needle and represented in a map legend.

## 4 Conclusions

This work presents an integrated multilayer topological model of the human body, the respective graphical UI, and functionalities that allow exploring in detail the human body. The final system characteristics result from the expansion of the input model in terms of the linear geometric component and from the neighborhood topology and connectivity

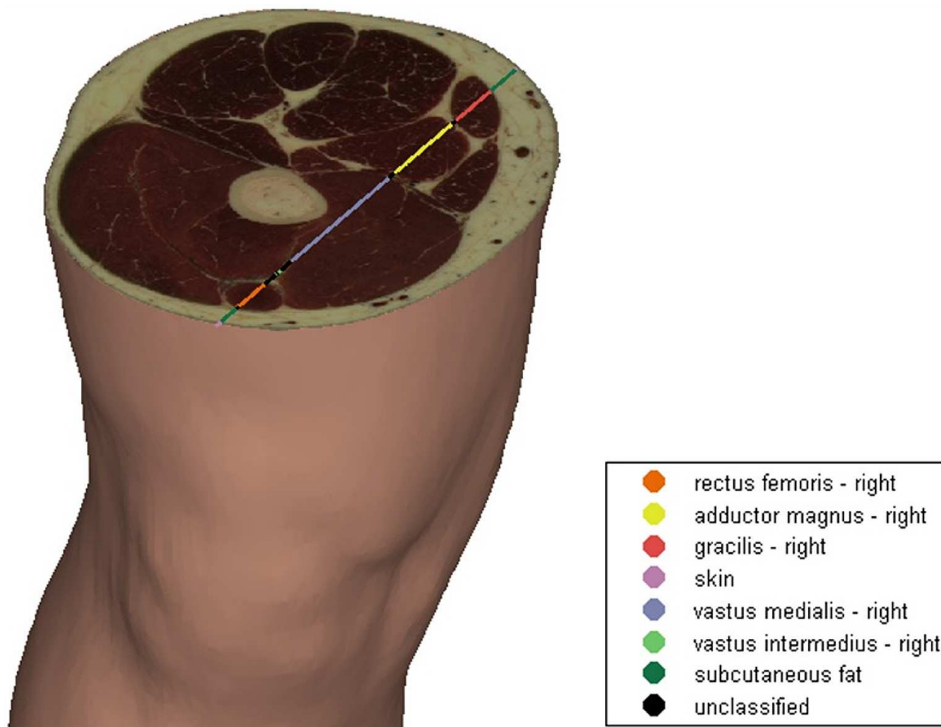


Figure 14: Inclusion analysis with the multilayered data.

components. New functionalities were made available in the graphical interface, especially the editing, identification, spatial analysis, and measurement functionalities.

The information of anatomical atlases is typically provided through the identification functions that allow for directly recognizing the anatomical structures and selected sub-regions, and for connecting to local documents or web pages. The functionalities that are unusually available in anatomical atlas are primarily related to the GIS component in which this new system is based. The GIS concepts from which the system was developed are related to the three-dimensional topological digital model and to the graphical interface with multilayer management and analysis functionalities that use the model topology.

The verification of the proper functioning of the various tools was carried out by analyzing the results. In the case of the metrics tools, this analysis consisted of a comparison with reference values published in scientific papers. The identification, spatial analysis, view, and navigation tools were assessed by their direct use, which leads to known results.

The use and the tests performed with the graphical UI tools allowed for validating the system and verifying its ability to reproduce the information provided in the anatomical atlas. Some limitations of traditional anatomical atlases were overcome, such as the interactive exploration of the human body and the completion of measurement and spatial analysis operations.



## Acknowledgements

The authors acknowledge the contribution of the U.S. National Library of Medicine for making available the datasets used in this work.

## References

- [1] AGUR, A. M. R., DALLEY, A. F., AND GRANT, J. C. B. *Grant's Atlas of Anatomy*. Wolters Kluwer Health/Lippincott Williams & Wilkins, 2013.
- [2] ARGOSY PUBLICATIONS. Visible Body. <http://www.visiblebody.com/index.html>, 2008. Last Accessed June 20, 2015.
- [3] ATILA, U., KARAS, I. R., AND ABDUL-RAHMAN, A. A 3D-GIS implementation for realizing 3D network analysis and routing simulation for evacuation purpose. In *Lecture Notes in Geoinformation and Cartography*. Springer, 2013, pp. 249–260. doi:10.1007/978-3-642-29793-9-14.
- [4] BARBEITO, A., CABRAL, P., PAINHO, M., AND O'NEILL, J. G. An integrated model of the human body. In *Proc. Portuguese Association for Information Systems (CAPSI) 14th Conference on Health Information Systems (2014)*.
- [5] BARBEITO, A., PAINHO, M., CABRAL, P., AND O'NEILL, J. G. A topological multilayer model of the human body. *Geospatial Health* 10, 2 (2015), 199–204. doi:10.4081/gh.2015.375.
- [6] BIODIGITAL HUMAN. Biodigital Human. <http://human.biodigital.com/index.html>, 2013. Last Accessed June 20, 2015.
- [7] BRASEBIN, M., PERRET, J., MUSTIÈRE, S., AND WEBER, C. Measuring the impact of 3D data geometric modeling on spatial analysis: Illustration with Skyview factor. *Usage, Usability, and Utility of 3D City Models – European COST Action TU0801 02001* (2012). doi:10.1051/3u3d/201202001.
- [8] BURCHIANTI, L., BARROS, M., AND CURCIO, D. Illustrations, CT scans and pictures of anatomical dissections in a 3D atlas of the human hand. *The FASEB Journal* 29, 1 Supplement (2015).
- [9] CAON, M. Voxel-based computational models of real human anatomy: A review. *Radiation and Environmental Biophysics* 42, 4 (2004), 229–235. doi:10.1007/s00411-003-0221-8.
- [10] CONTI, J. File Exchange - MATLAB Central. <http://www.mathworks.com/matlabcentral/fileexchange/>, 2004. Last Accessed June 20, 2015.
- [11] CORNEA, N. D., AND MIN, P. Curve-skeleton properties, applications, and algorithms. *IEEE Transactions on Visualization and Computer Graphics* 13, 3 (2007), 530–548. doi:http://dx.doi.org/10.1109/TVCG.2007.1002

- [12] CSENDES, A., AND BURGOS, A. M. Size, volume and weight of the stomach in patients with morbid obesity compared to controls. *Obesity Surgery* 15, 8 (2005), 1133–1136. doi:10.1381/0960892055002158.
- [13] CURTIS, H., AND BARNES, N. S. *Invitation to Biology*. W. H. Freeman, 1994.
- [14] DATABASE CENTER FOR LIFE SCIENCE. BodyParts3D. <http://lifesciencedb.jp/bp3d/>, 2009. Last Accessed June 20, 2015.
- [15] DIJKSTRA, E. W. A note on two problems in connexion with graphs. *Numerische Mathematik* 1, 1 (1959), 269–271. doi:10.1007/BF01386390.
- [16] DIXON, A. K., BOWDEN, D. J., ELLIS, H., AND LOGAN, B. M. *Human Sectional Anatomy: Atlas of Body Sections, CT and MRI Images, Fourth Edition*. Taylor & Francis, 2014.
- [17] FELDESMAN, M. R., KLECKNER, J. G., AND LUNDY, J. K. Femur/stature ratio and estimates of stature in mid- and late-Pleistocene fossil hominids. *American Journal of Physical Anthropology* 83, 3 (1990), 359–72. doi:10.1002/ajpa.1330830309.
- [18] GARB, J. L., GANAI, S., SKINNER, R., BOYD, C. S., AND WAIT, R. B. Using GIS for spatial analysis of rectal lesions in the human body. *International Journal of Health Geographics* 6 (2007), 11. doi:10.1186/1476-072X-6-11.
- [19] HOPPE, H., DEROSE, T., DUCHAMP, T., McDONALD, J., AND STUETZLE, W. Surface reconstruction from unorganized points. *ACM SIGGRAPH Computer Graphics* 26, 2 (1992), 71–78. doi:10.1145/142920.134011.
- [20] HUMAN GENETICS UNIT MEDICAL RESEARCH COUNCIL. eMouse Atlas. <http://www.emouseatlas.org>.
- [21] JASIKA, N., ALISPAHIC, N., ELMA, A., ILVANA, K., ELMA, L., AND NOSOVIC, N. Dijkstra's shortest path algorithm serial and parallel execution performance analysis. In *Proc. 35th International Convention MIPRO (2012)*, IEEE, pp. 1811–1815.
- [22] KAN, M. K., AND HOPKINS, G. B. Measurement of liver volume by emission computed tomography. *Journal of Nuclear Medicine* 20, 6 (1979), 514–20.
- [23] KRÄMER, M., AND STEIN, A. Automated urban management processes: Integrating a graphical editor for modular domain-specific languages into a 3D GIS. In *Proc. 19th International Conference on Urban Planning and Regional Development in the Information Society GeoMultimedia (2014)*.
- [24] LIU, G., ZHU, Q., HE, Z. W., ZHANG, Y. T., WU, C. L., LI, X. M., AND WENG, Z. P. 3D GIS database model for efficient management of large scale underground spatial data. In *Proc. 17th International Conference on Geoinformatics, Vols 1 and 2*, L. Di and A. Chen, Eds. IEEE, New York, 2009, pp. 754–758.
- [25] MAI, J. K., MAJTANIK, M., AND PAXINOS, G. *Atlas of the Human Brain*. Elsevier Science, 2015.

- [26] MARTONE, M. E., ZASLAVSKY, I., GUPTA, A., MEMON, A., TRAN, J., WONG, W., FONG, L., LARSON, S. D., AND ELLISMAN, M. H. The smart atlas: Spatial and semantic strategies for multiscale integration of brain data. In *Anatomy Ontologies for Bioinformatics*, A. Burger, D. Davidson, and R. Baldock, Eds., vol. 6. Springer, 2008, pp. 267–286.
- [27] MICLAUS, G. D., AND PLES, H. *Atlas of CT Angiography Normal and Pathologic Findings*. Springer International Publishing, 2014.
- [28] MOSTELLER, R. D. Simplified calculation of body-surface area. *New England Journal of Medicine* 317, 17 (1987), 1098–1098. doi:10.1056/NEJM198710223171717.
- [29] PARK, J. S., CHUNG, M. S., HWANG, S. B., SHIN, B. S., AND PARK, H. S. Visible Korean human: Its techniques and applications. *Clinical Anatomy* 19, 3 (2006), 216–224.
- [30] PAXINOS, G. *The Mouse Brain in Stereotaxic Coordinates*. Gulf Professional Publishing, 2004.
- [31] PICKLE, L. W., SZCZUR, M., LEWIS, D. R., AND STINCHCOMB, D. G. The crossroads of GIS and health information: A workshop on developing a research agenda to improve cancer control. *International Journal of Health Geographics* 5, 1 (nov 2006), 51. doi:10.1186/1476-072X-5-51.
- [32] PILOUK, M. *Integrated Modelling for 3D GIS*. PhD thesis, Enschede, 1996.
- [33] RICCIARDI, A. Thieme atlas of anatomy: General anatomy and musculoskeletal system. *The Yale Journal of Biology and Medicine* 88, 1 (2015), 100.
- [34] RICHARDSON, D. B., VOLKOW, N. D., KWAN, M., KAPLAN, R., GOODCHILD, M. F., AND CROYLE, R. T. Spatial turn in health research. *Science* 339, 6126 (2013), 1390–1392.
- [35] RICHARDSON, L., VENKATARAMAN, S., STEVENSON, P., YANG, Y., MOSS, J., GRAHAM, L., BURTON, N., HILL, B., RAO, J., BALDOCK, R. A., AND ARMIT, C. EMAGE mouse embryo spatial gene expression database: 2014 update. *Nucleic Acids Research* 42, D1 (2014), D835–D844. doi:10.1093/nar/gkt1155.
- [36] RINEHART, H., AND STAFF, W. *Holt Biology: Visualizing Life: Teaching Resources*. Holt McDougal, 1998.
- [37] SCHUMM, M., SCHLICH, M., AND SCHLICH, E. 3D-body-scan als Anthropometrisches Verfahren zur Bestimmung der Spezifischen Körperoberfläche. *Ernährungs Umschau* 57, 4 (2010), 178–183.
- [38] SPITZER, V., ACKERMAN, M. J., SCHERZINGER, A. L., AND WHITLOCK, D. The visible human male: A technical report. *Journal American Medical Informatics Association* 3, 2 (1996), 118–130.
- [39] SPRATT, J. D., SALKOWSKI, L. R., WEIR, J., AND ABRAHAMS, P. H. *Imaging Atlas of Human Anatomy*. Elsevier Health Sciences UK, 2010.
- [40] STRECKER, W., KEPPLER, P., GEBHARD, F., AND KINZL, L. Length and torsion of the lower limb. *The Journal of Bone and Joint Surgery* 79, 6 (1997), 1019–1023.

- [41] SUWARDHI, D. 3D geo-database implementation using craniofacial geometric morphometrics database system. In *Innovations in 3D Geo Information Systems*, A. Abdul-Rahman, S. Zlatanova, and V. Coors, Eds. Springer, 2006, pp. 279–294.
- [42] TEGTMEIER, W., ZLATANOVA, S., VAN OOSTEROM, P. J. M., AND HACK, H. R. G. K. 3D-GEM: Geo-technical extension towards an integrated 3D information model for infrastructural development. *Computers and geosciences* 64 (2014), 126–135. doi:<http://dx.doi.org/10.1016/j.cageo.2013.11.003>.
- [43] TOLTECH. VH Dissector for Medical Education. <http://www.toltech.net/anatomy-software/solutions/vh-dissector-for-medical-education>, 2014. Last Accessed June 20, 2015.
- [44] UNGAR, P. S., AND M'KIRERA, F. A solution to the worn tooth conundrum in primate functional anatomy. *Proceedings of the National Academy of Sciences* 100, 7 (2003), 3874–3877. doi:10.1073/pnas.0637016100.
- [45] VERBRAECKEN, J., VAN DE, H. P., DE BACKER, W., AND VAN GAAL, L. Body surface area in normal-weight, overweight, and obese adults. A comparison study. *Metabolism* 55, 0026-0495 (Print) (2006), 515–524.
- [46] WAN, Y., LEWIS, A. K., COLASANTO, M., VAN LANGEVELD, M., KARDON, G., AND HANSEN, C. A practical workflow for making anatomical atlases for biological research. *IEEE Computer Graphics and Applications* 32, 5 (2012), 70–80. doi:10.1109/MCG.2012.64.
- [47] WENZEL, V., IDRIS, A. H., BANNER, M. J., KUBILIS, P. S., BAND, R., WILLIAMS, J. L., AND LINDNER, K. H. Respiratory system compliance decreases after cardiopulmonary resuscitation and stomach inflation: Impact of large and small tidal volumes on calculated peak airway pressure. *Resuscitation* 38, 2 (1998), 113–118.
- [48] WOODFORD, O. File Exchange - MATLAB Central. <http://www.mathworks.com/matlabcentral/fileexchange/>, 2011.
- [49] WORLD HEALTH ORGANIZATION. BMI classification 2013. <http://apps.who.int/bmi/index.jsp>, 2013.
- [50] ZASLAVSKY, I., BALDOCK, R. A., AND BOLINE, J. Cyberinfrastructure for the digital brain: Spatial standards for integrating rodent brain atlases. *Frontiers in Neuroinformatics* 8, 74 (2014).
- [51] ZASLAVSKY, I., HE, H., TRAN, J., MARTONE, M., AND GUPTA, A. Integrating brain data spatially: Spatial data infrastructure and atlas environment for online federation and analysis of brain images. In *Proc. 15th International Workshop on Database and Expert Systems Applications* (2004), IEEE, pp. 389–393. doi:10.1109/DEXA.2004.1333505.
- [52] ZHANG, S. X., HENG, P. A., AND LIU, Z. J. Chinese visible human project. *Clinical Anatomy* 19, 3 (2006), 204–215. doi:10.1002/ca.20273.
- [53] ZINECKER, C., HIRSCH, M. C., KRAMER, T., HARDER, B., HAGEMANN, T., KRASOWSKI, C., SCHÄFER, C., TURTIAINEN, M., AND GAUER, M. *Neuroanatomy: 3D-Stereoscopic Atlas of the Human Brain*. Springer London, Limited, 2012.

- [54] ZYGOTE BODY MEDIA. Zygote Body. <http://zygotebody.com/>, 2011. Last Accessed April 25, 2015.